Supplemental material to "Linear temperature dependence of intrinsic resistivity of metals determined solely by singular electronic structure"

Shuo Zhao,[1] Mingfeng Zhu,[1,*] and Yisong Zheng[1,†]

[1] *Key Laboratory of Physics and Technology for Advanced Batteries (Ministry of Education) and Department of Physics, Jilin University, Changchun 130012, China.*

In this supplemental material, we firstly provide the technical details of the first-principles calculations for calculating the electronic, phononic structures and the electron-phonon interaction (EPI) matrix elements of rhombohedral trilayer graphene (RTG). Subsequently, we introduce the tight-binding (TB) Hamiltonian and the deformation potential (DP) model of RTG. Thirdly, we formulate the iterative algorithm for solving the Boltzmann transport equation (BTE), in order to calculate the intrinsic resistivity of RTG. Finally, we make a comparison between the intrinsic resistivity of RTG obtained from first-principles calculations and that obtained using the TB Hamiltonian combined with the DP model.

I. THE TECHNIQUE DATAILS OF THE FIRST-PRINCIPLES CALCULATIONS

To perform the first-principles calculations on the intrinsic resistivity of RTG, we obtain the energy band and the phonon dispersion in the theoretical framework of Density Functional Theory (DFT)[1] and Density Functional Perturbation Theory [2], respectively, using the Quantum ESPRESSO software package[3, 4]. The Generalised Gradient Approximation of Perdew-Burke-Ernzerhof functional[5] is used for the exchange-correlation potential and the Troullier-Martins norm-conserving pseudopotential[6] is chosen to incorporate the interaction between the valence electronic and the ion cores. The kinetic energy cutoff for wavefunctions is set to 150 Ry and the semiempirical Grimme's DFT-D2 model[7, 8] is used to describe the interlayer coupling. Then, a $32 \times 32 \times 1$ Monkhorst Pack grid is used for the k-point smapling in the Brillouin zone for the electronic structure calculations, while an $8 \times 8 \times 1$ grid of q points is used for the phonon calculations. Actually, such k- and q-point meshes are too coarse for the numerical calculation of the intrinsic resistivity, since only very sparse k-points fall in the vicinity of the Fermi surface. Consequently, it is almost impossible to get a converging result of the intrinsic resistivity. In particular, in the case of RTGs, the size of the Fermi surface is very small. Therefore, this problem is particularly severe. However, first-principles calculations on a much finer k-mesh or q-mesh imply huge computational burden. To circumvent such a prohibitive task, we adopt the Wannier interpolation approach, realized by the EPW code[9], which allows affordable and accurate calculations of the electron and phonon energy spectra as well as the EPI matrix elements on ultrafine k-mesh and q-mesh. Then, with these quantities as the input, we calculate the intrinsic resistivity of RTG by solving the BTE iteratively, as depicted in Section III.

II. THE TIGHT-BINDING HAMILTONIAN AND DEFORMATIONAL POTENTIAL MODEL OF RTG

Although we can obtain the electronic band structure of RTG through the first-principles calculations as introduced above, a simple Hamiltonian established by a limited number of parameters in the framework of TB model can reproduce the band structure of RTG obtained by the first-principles calculations with satisfactory precision. It is well-known that the electronic structure of RTG is characterized by the two energy-degenerate valleys located around K and K' points (two inequivalent corners of the hexagonal Brillouin zone), similar to the case of monolayer graphene. Around either of these valleys, the TB Hamiltonian can be parameterized in the form of following matrix[10].

$$H = \begin{bmatrix} \Delta_2+\delta & \gamma_2/2 & v_0\bar{k} & v_4\bar{k} & v_3 k & 0 \\ \gamma_2/2 & \Delta_2+\delta & 0 & v_3\bar{k} & v_4 k & v_0 k \\ v_0 k & 0 & \Delta_2 & \gamma_1 & v_4\bar{k} & 0 \\ v_4 k & v_3 k & \gamma_1 & -2\Delta_2 & v_0\bar{k} & v_4\bar{k} \\ v_3 k & v_4\bar{k} & v_4 k & v_0 k & -2\Delta_2 & \gamma_1 \\ 0 & v_0\bar{k} & 0 & v_4 k & \gamma_1 & \Delta_2 \end{bmatrix} \tag{1}$$

* Corresponding author: mfzhu@jlu.edu.cn
† Corresponding author: zhengys@jlu.edu.cn

where $k = a(\xi k_x + ik_y)$ and $\bar{k} = a(\xi k_x - ik_y)$ are the dimensionless, valley-dependent momenta for valley $\xi \in \{\pm\}$, and a is the relaxed lattice constant of RTG. The parameters take the following values (all quantities in units of eV): $\Delta_2 = -0.0023$, $\delta = -0.0105$, $\gamma_0 = 3.1$, $\gamma_1 = 0.38$, $\gamma_2 = -0.015$, $\gamma_4 = -0.141$, and $v_i = \gamma_i\sqrt{3}/2$. It should be noted that the basis (Bloch orbitals) for this matrix correspond to the atoms 1A, 3B, 1B, 2A, 2B, 3A, where A and B corresponds to sublattices, and 1, 2 and 3 correspond to layers, as shown in Fig.1(a) in the main text.

In terms of the DP model[11], which only takes into account the interaction between the electron and longitudinal acoustic (LA) phonon, the modulus square of EPI matrix element that appears in the BTE takes a very simple form,

$$|g^{\nu}_{mn}(\boldsymbol{k}, \boldsymbol{q})|^2 = |g_{\boldsymbol{q}}|^2 = Dq \tag{2}$$

where the parameter $\tilde{D}$ involves the so-called DP model parameter, phonon velocity and the mass density. Consistent with the value reported in Ref.[12], we use $D = 3.94 \times 10^{-3}$ eV·Å. In addition, the frequency of the LA phonon follows a linear dispersion, given by $\omega(q) = cq$ with the phonon velocity $c = 2.94 \times 10^5$ m/s.

III. ITERATION METHOD

With the above parameterized model, we can estimate rapidly the intrinsic resistivity of RTG, instead of the first-principles calculations. Prior to presenting the numerical results, we would like to make a simple supplement to the BTE. As described in the main text, the BTE is approximately solved using energy relaxation time approximation (ERTA). In fact, we can numerically solve the BTE in term of iteration algorithm, beyond the ERTA. In so doing, we can write down the BTE in an iterative form as[13]

$$F^{i+1}_{n\boldsymbol{k}} = v_{n\boldsymbol{k}}\tau_{n\boldsymbol{k}} + \frac{\tau_{n\boldsymbol{k}}}{f^0_{n\boldsymbol{k}}(1 - f^0_{n\boldsymbol{k}})} \sum_{\nu\boldsymbol{q}m} P_{n\boldsymbol{k},m\boldsymbol{k}+\boldsymbol{q}} F^i_{m\boldsymbol{k}+\boldsymbol{q}} \tag{3}$$

where $F_{n\boldsymbol{k}}$ has the meaning of mean free path which is obtained by the iteration procedure as illustrated by the above equation with the initial value of the mean free path is set as $F^0_{n\boldsymbol{k}} = v_{n\boldsymbol{k}}\tau_{n\boldsymbol{k}}$. Note the superscripts i+1 and i of the mean free path denotes the steps of the iteration procedure. When the difference of the mean free path between the adjacent step of iteration is smaller than a certain threshold, we obtain the convergent value of the mean free path. In the above equation,

$$\begin{aligned} P_{n\boldsymbol{k},m\boldsymbol{k}+\boldsymbol{q}} =& \frac{2\pi}{\hbar} \sum_{\nu} |g^{\nu}_{mn}(\boldsymbol{k}, \boldsymbol{q})|^2 f^0_{n\boldsymbol{k}}(1 - f^0_{m\boldsymbol{k}+\boldsymbol{q}}) \\ & [(n_q + 1)\delta(\epsilon_{n\boldsymbol{k}} - \hbar\omega_{\nu\boldsymbol{q}} - \epsilon_{m\boldsymbol{k}+\boldsymbol{q}}) + n_q\delta(\epsilon_{n\boldsymbol{k}} + \hbar\omega_{\nu\boldsymbol{q}} - \epsilon_{m\boldsymbol{k}+\boldsymbol{q}})] \end{aligned} \tag{4}$$

Finally, the intrinsic resistivity is expressed in terms of the numerical results of the mean free path, due to its small anisotropy, we only calculated the resistivity along the armchair direction

$$\rho = \left[\frac{2e^2}{NVk_BT} \sum_{n\boldsymbol{k}} f^0_{n\boldsymbol{k}}(1 - f^0_{n\boldsymbol{k}}) \boldsymbol{v}_{n\boldsymbol{k}} F_{n\boldsymbol{k}} \right]^{-1} \tag{5}$$

In contrast to Eq.(1) in the main text, i.e. the intrinsic resistivity calculated using the ERTA, the iteration solution of the BTE can provide a more accurate intrinsic resistivity, taking into account at least the effect of large-angle scattering weight.

IV. JUSTIFICATION OF THE APPROXIMATION USING THE AVERAGED RELAXATION TIME IN THE RESISTIVITY EXPRESSION

In order to verify the validity of Eq.(3) in the main text, we calculated $\tau_{n\boldsymbol{k}}/\tau$ for different k points as shown in Fig.1, and we can see that even if the Fermi energy level is near a singularity, the $\tau_{n\boldsymbol{k}}$ does not vary in a drastic manner. We also calculated the standard deviation of them, and we can see that the standard deviation is small regardless of the presence of a singularity near the Fermi energy level, so it is reasonable for us to approximate $\tau_{n\boldsymbol{k}}$ by the mean value $\bar{\tau}$. From this result we can further infer that the el-ph interaction matrix elements do not vary sensitively with electronic energy even in the vicinity of drastically varying region of the band, which is unlike the energy-resolved electronic velocity squared shown in Fig.1a.

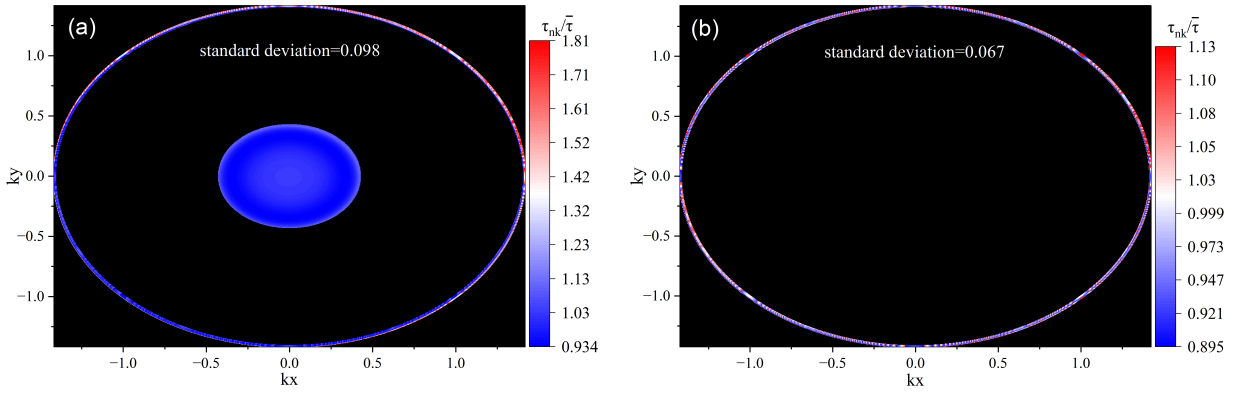

FIG. 1. Different colours in the figure indicate the magnitude of for different k. The Fermi energy level is selected at -0.012 eV (a) and 0.122 eV (b), respectively, the same as that in Fig.1 in the main text.

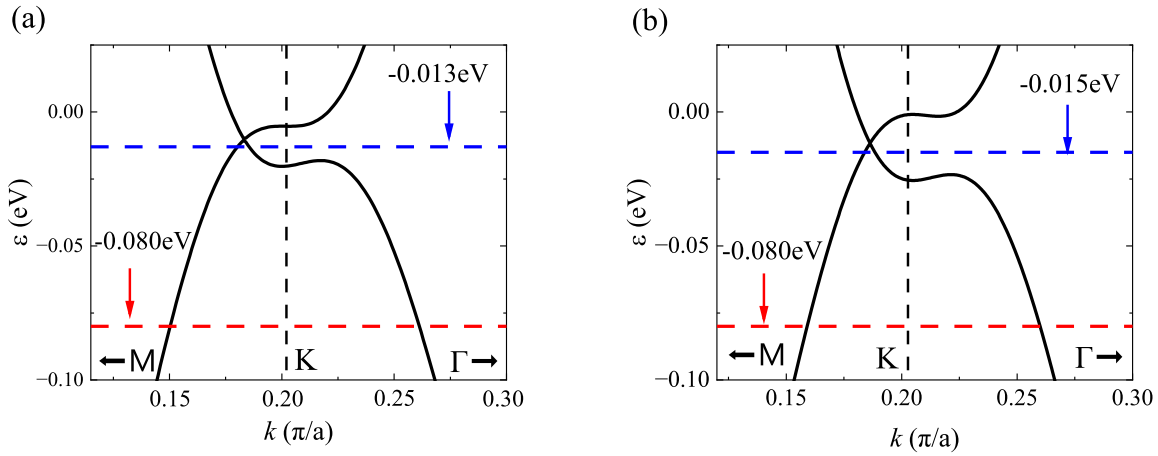

FIG. S2. (a) The energy band of RTG obtained from calculations using the TB Hamiltonian model. We mark the positions of $\epsilon_F = -0.013$ and -0.08 eV with blue and red lines, respectively. (b) a replot of Fig.2(b) in the main text, the energy band of first principles calculations

V. RESULTS AND DISCUSSIONS

The crystal structure of RTG is shown in Fig. 2(a) in the main text. The optimized bond length (lattice constant) and interlayer distance are 1.42(2.45)Å and 3.24Å, respectively, which agree with previous literature[14]. The unusual band structure of RTG around K valley, obtained by the first-principles calculations, has been shown in Fig.3(a) in the main text. The electronic band structure is characterized by triple Dirac points and a local flat band among them. Such a band feature can be well reproduced by the TB Hamiltonian. In Fig.S2, we compare the local dispersions of the band energy in K valley, calculated by the first-principles calculations and the TB Hamiltonian. We can see that both results agree with each other very well, except for the trivial differences. In Ref.[14], the authors selected several typical energy points, of which we use two representative ones as labeled in Fig.2(a). We use the two Fermi energies to calculate the corresponding intrinsic resistivity as a function of temperature. What is interesting is that the two typical Fermi levels correspond just to Fermi surfaces with distinct topology, as shown in Fig.3(a). In other words, when shifting the Fermi level within such an energy range, the Fermi surface undergoes the so-called Lifshitz transition, i.e. a topological variation of the Fermi surface geometry. As seen from Fig.3(b), the Lifshitz transition of the Fermi surface can also be observed in the result of the first-principles calculations, similar to the case of TB model.

In Fig.4(a), we show the numerical results of the intrinsic resistivities as functions of temperature calculated by means of TB Hamiltonian plus DP model. Firstly, we can see that the resistivity exhibits a linear ρ-T relationship at a critical temperature of 500 K, which is much higher than $T_{BG} = 50$ K when the Fermi energy is located near

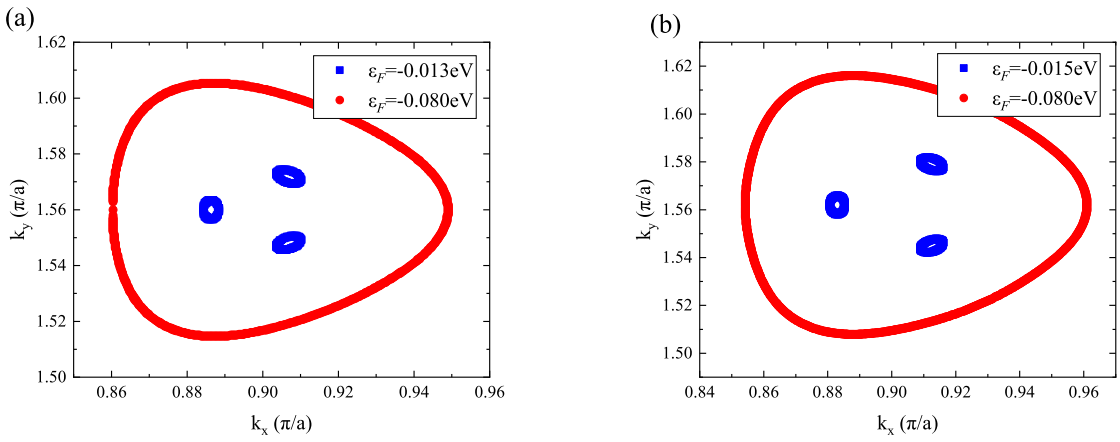

FIG. S3. Fermi surfaces calculated using (a) the TB Hamiltonian model and (b) the first-principles calculations with $\epsilon_F = -0.013$ eV and -0.08 eV.

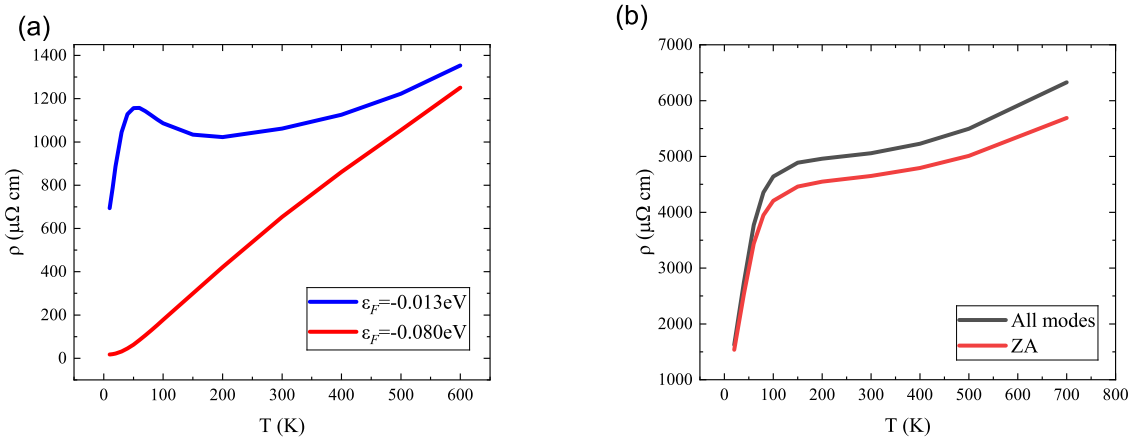

FIG. S4. (a) ρ-T curves calculated by using the TB Hamiltonian and the DP model, with blue for $\epsilon_F = -0.013$ eV and red for $\epsilon_F = -0.08$ eV. (b) Resistivity contributed by the out-of-plane flexural (ZA) phonons (red) and the resistivity contributed by all phonon branches (black) obtained from the first-principles calculations.

the flat band ($\epsilon_F = -0.013$ eV). On the contrary, the resistivity depends linearly on temperature at a much lower critical temperature when the Fermi level is far away from the local flat band ($\epsilon_F = -0.080$ eV). It is very similar to the intrinsic resistivities calculated by the first-principles calculations, as shown in Fig.3(a) in the main text. Such a common feature of the temperature dependent resistivities calculated in both methods is just due to the fact that the linear ρ-T relationship is determined by T_e when the Fermi level is near the flat band.

Despite the aforementioned common feature of the ρ-T curves obtained by the two different numerical approaches, we can find that the intrinsic resistivity obtained by the first-principles calculations is significantly larger than the one calculated using TB plus DP model. By calculating the phonon branch resolved resistivity using first-principles calculations, we find that it is the out-of-plane flexural (ZA) phonon, rather than the LA phonon, that plays the leading role in contributing to the intrinsic resistivity as shown in Fig.4(b). Considering the much lower frequency and hence the much larger population of the ZA phonons compared to those of LA phonons as seen in Fig.2(d) in the main text, it is not surprising that the first-principles calculations yields a much larger intrinsic resistivity in comparison with the one obtained from the DP model which considers only LA phonons. In addition, the frequencies of ZA phonons do not linearly depend on $\boldsymbol{q}$ which also causes the DP model to fail in this scenario. Such a result indicates that the DP model is not adequate to provide a quantitative description of the intrinsic resistivity, even though the physical parameters in the DP model is adopted from previous experimental or theoretical works concerning graphite or graphene monolayers. In other words, those parameters are not competent to RTG. But the DP model does not

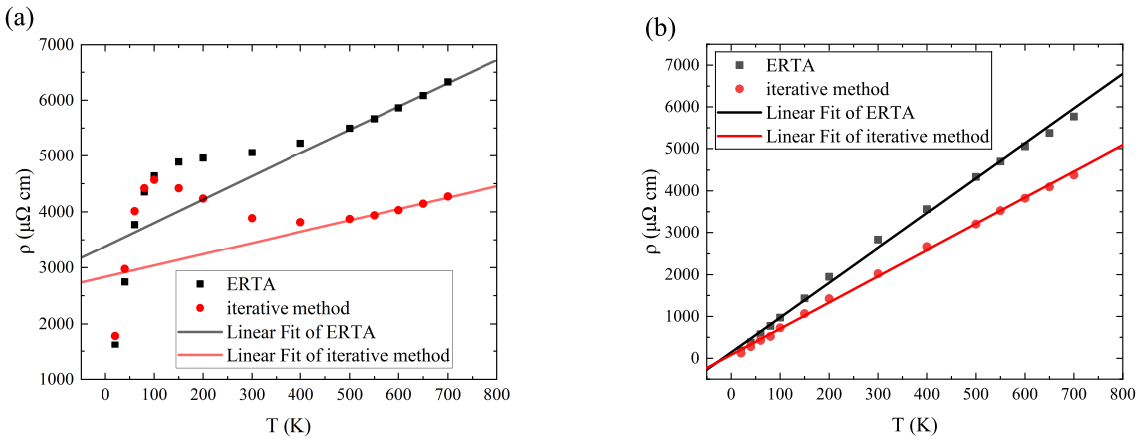

FIG. S5. The ρ-T curves obtained by the iterative method (red) and the ones calculated in the Energy relaxation time approximation (black) using the first-principles calculations with $\epsilon_F = -0.015$ eV (a) and $\epsilon_F = -0.080$ eV (b).

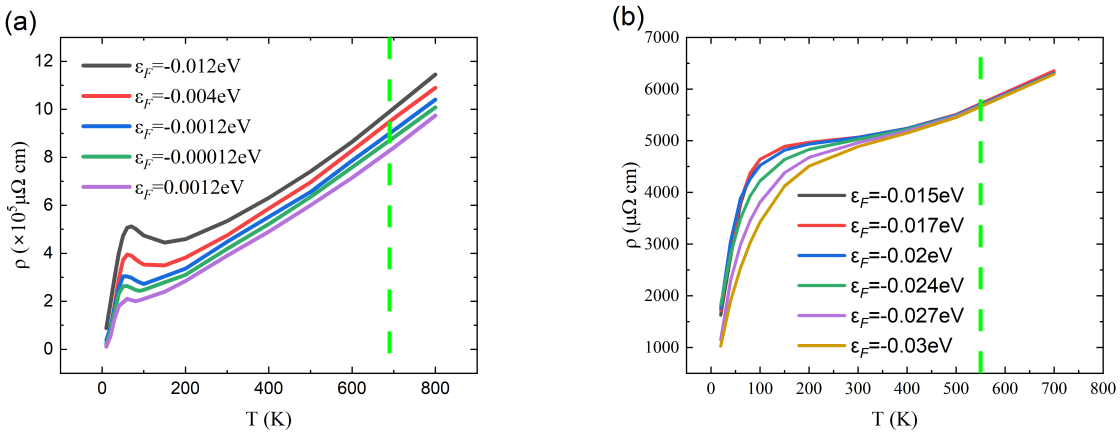

FIG. S6. Resistivity-temperature curves at different Fermi levels of (a) Mexican hat energy band and (b) RTG(under ERTA). We use green dashed line to point out the T_e in both figure.

affect T_e to manifest itself in determining the linear temperature dependence of the intrinsic resistivity of RTG because the TB Hamiltonian can well reproduce the electronic structure of RTG using the first-principles calculations.

It is necessary to make a comparison between the results of the intrinsic resistivities obtained by ERTA and iteration solution of BTE. The numerical results are shown in Fig.S5. It can be seen that when the Fermi energy is close to the flat band, although the iterative method introduces a significant correction to the results of ERTA, the onset temperature of the linear ρ-T relationship remains unchanged. This further confirms that the onset temperature of the linear ρ-T relationship is governed by T_e, which is almost unaffected by the large-angle scattering of electrons by phonons through EPI as taken into account by the iterative method.

Finally, from the ρ-T curves shown in Fig.S4 and Fig.5(a) where the Fermi level is in the vicinity of local flat band(also near the electric neutrality point), we can find that the resistivity calculated by TB model exhibits a relatively flat feature in the temperature range from 100 to 400K. When $T > T_e$, the ρ-T curves begin to be linear. At the low temperature side of the flat region there is a peak. But the appearance of such a peak depends on the numerical method. For example, as shown in Fig.5(a), the relaxation time approximation can not yield such a peak. We stress herein that a similar flattening of resistivity was also found previously in Ref.[14], with some differences in details, such as the degree of flatness and temperature range of the flat region. These differences arise from the calculation methods and model parameters. We then calculate the ρ-T curves at various Fermi energies near the flat band in both our toy model and RTG, as shown in Fig.S6. It can be seen that as the Fermi level gradually decreases

(moving away from the flat band), the influence of the electronic structure on the ρ–T relation weakens. Nevertheless, regardless of how Fermi energy changes, once $T > T_e$, the constraint imposed by the electronic structure on the linear ρ–T behavior can safely be neglected. Although a Fermi-level-dependent characteristic temperature has not been explicitly defined here, such a quantity can be extracted from the $TZ(T) \sim T$ relation.

REFERENCE

[1] W. Kohn and L. J. Sham. Self-consistent equations including exchange and correlation effects. *Phys. Rev.*, 140:A1133–A1138, Nov 1965.

[2] Stefano Baroni, Stefano de Gironcoli, Andrea Dal Corso, and Paolo Giannozzi. Phonons and related crystal properties from density-functional perturbation theory. *Rev. Mod. Phys.*, 73:515–562, Jul 2001.

[3] Paolo Giannozzi, Stefano Baroni, Nicola Bonini, Matteo Calandra, Roberto Car, Carlo Cavazzoni, Davide Ceresoli, Guido L Chiarotti, Matteo Cococcioni, Ismaila Dabo, Andrea Dal Corso, Stefano de Gironcoli, Stefano Fabris, Guido Fratesi, Ralph Gebauer, Uwe Gerstmann, Christos Gougoussis, Anton Kokalj, Michele Lazzeri, Layla Martin-Samos, Nicola Marzari, Francesco Mauri, Riccardo Mazzarello, Stefano Paolini, Alfredo Pasquarello, Lorenzo Paulatto, Carlo Sbraccia, Sandro Scandolo, Gabriele Sclauzero, Ari P Seitsonen, Alexander Smogunov, Paolo Umari, and Renata M Wentzcovitch. Quantum espresso: a modular and open-source software project for quantum simulations of materials. *Journal of Physics: Condensed Matter*, 21(39):395502, sep 2009.

[4] P Giannozzi, O Andreussi, T Brumme, O Bunau, M Buongiorno Nardelli, M Calandra, R Car, C Cavazzoni, D Ceresoli, M Cococcioni, N Colonna, I Carnimeo, A Dal Corso, S de Gironcoli, P Delugas, R A DiStasio, A Ferretti, A Floris, G Fratesi, G Fugallo, R Gebauer, U Gerstmann, F Giustino, T Gorni, J Jia, M Kawamura, H-Y Ko, A Kokalj, E Küçükbenli, M Lazzeri, M Marsili, N Marzari, F Mauri, N L Nguyen, H-V Nguyen, A Otero de-la Roza, L Paulatto, S Poncé, D Rocca, R Sabatini, B Santra, M Schlipf, A P Seitsonen, A Smogunov, I Timrov, T Thonhauser, P Umari, N Vast, X Wu, and S Baroni. Advanced capabilities for materials modelling with quantum espresso. *Journal of Physics: Condensed Matter*, 29(46):465901, oct 2017.

[5] John P. Perdew, Kieron Burke, and Matthias Ernzerhof. Generalized gradient approximation made simple. *Phys. Rev. Lett.*, 77:3865–3868, Oct 1996.

[6] John P. Perdew and Yue Wang. Accurate and simple analytic representation of the electron-gas correlation energy. *Phys. Rev. B*, 45:13244–13249, Jun 1992.

[7] Stefan Grimme. Semiempirical gga-type density functional constructed with a long-range dispersion correction. *Journal of Computational Chemistry*, 27(15):1787–1799, 2006.

[8] Vincenzo Barone, Maurizio Casarin, Daniel Forrer, Michele Pavone, Mauro Sambi, and Andrea Vittadini. Role and effective treatment of dispersive forces in materials: Polyethylene and graphite crystals as test cases. *Journal of Computational Chemistry*, 30(6):934–939, 2009.

[9] S. Poncé, E.R. Margine, C. Verdi, and F. Giustino. Epw: Electron–phonon coupling, transport and superconducting properties using maximally localized wannier functions. *Computer Physics Communications*, 209:116–133, 2016.

[10] Fan Zhang, Bhagawan Sahu, Hongki Min, and A. H. MacDonald. Band structure of *abc*-stacked graphene trilayers. *Phys. Rev. B*, 82:035409, Jul 2010.

[11] J. Bardeen and W. Shockley. Deformation potentials and mobilities in non-polar crystals. *Phys. Rev.*, 80:72–80, Oct 1950.

[12] Yang-Zhi Chou, Fengcheng Wu, Jay D. Sau, and Sankar Das Sarma. Acoustic-phonon-mediated superconductivity in moiréless graphene multilayers. *Phys. Rev. B*, 106:024507, Jul 2022.

[13] Wu Li. Electrical transport limited by electron-phonon coupling from boltzmann transport equation: An ab initio study of si, al, and mos_2. *Phys. Rev. B*, 92:075405, Aug 2015.

[14] Seth M. Davis, Yang-Zhi Chou, Fengcheng Wu, and Sankar Das Sarma. Phonon-limited resistivity of multilayer graphene systems. *Phys. Rev. B*, 107:045426, Jan 2023.